Multi-layered coarse grid modelling in 2D urban flood simulations

Albert S. Chen[1], Barry Evans[2], Slobodan Djordjević[1], Dragan A. Savić[1]

[1] Centre for Water Systems, College of Engineering, Mathematics and Physical Sciences, University of Exeter, UK

[2] Department of Geography, College of Life and Environmental Sciences, University of Exeter, UK

Abstract

Regular grids are commonly used in 2D flood modelling due to wide availability of terrain models and low pre-processing required for input preparation. Despite advances in both computing software and hardware, high resolution flood modelling remains computationally demanding when applied to a large study area when the available time and resources are limited. Traditional grid coarsening approach may reduce not only the computing demands, but also the accuracy of results due to the loss of detailed information. To keep key features that affect flow propagation within coarse grid, the approach proposed and tested in this paper adopts multiple layers in flood modelling to reflect individual flow paths separated by buildings within a coarse grid cell. The cell in each layer has its own parameters (elevation, roughness, building coverage ratio, and conveyance reduction factors) to describe itself and the conditions at boundaries with neighbourhood cells. Results of tests on the synthetic case study and the real world urban area show that the proposed multi-layered approach greatly improves the accuracy of coarse grid modelling with an insignificant additional computing cost. The proposed approach has been tested in conjunction with the UIM model by taking the high resolution results as the benchmark. The implementation of the proposed multi-layered methodology to any regular grid based 2D model would be straightforward.

Keywords: building coverage ratio (BCR); conveyance reduction factors (CRFs); multi-layered flood modelling; urban inundation model (UIM)

Introduction

Urbanisation associated with economic growth, particularly in developing countries, has become a strong global trend in the past half century (United Nations, 2010). Nowadays, more than 50% of the world's population live in urban areas. This number is growing and projections show that nearly 70% of world population will be living in urban areas by 2050. Hazard risks and exposures increase rapidly in cities as a consequence of the concentration of population and wealth, exhaustion of resources, and changing environmental and human activities (Mitchell, 2003). In England, the Environment Agency (2009) estimated that around 3.8 million properties are susceptible to surface water flooding (pluvial flooding). Due to climate change, the likelihood of surface water flooding is rising because the central estimate of UKCP09 (the UK Climate Projections 2009) predicted that the rainfall in winter wettest days could increase by 10-30% by the 2080s over the majority of the UK (Jenkins et al., 2009). The Pitt Review (Pitt, 2008) highlighted the fact that flood modelling is crucial to understanding the increase of flood risk caused by climate change. This Review also indicated that, although the Environment Agency has advanced understanding and models for assessing the risk of flooding from rivers and coasts, the information related to surface water flood risk is still limited. There has been significant research into fluvial and coastal flooding and tools have been developed to analyse them, but models for pluvial flooding are less advanced. Therefore, modelling and better understanding of the risk of surface water flooding is needed urgently for flood risk management.

Two-dimensional (2D) surface flood modelling can provide abundant information about the dynamics of flooding, which may improve the flood risk management. However, the efficiency of 2D flood modelling has been one of the major challenges to modellers. The performance of existing 2D models varies significantly depending the choice of time steps and the number of iterations within each time step, the efficiency of numerical algorithms,

the use of multi-processing, the hardware specification and other computational overhead costs for modelling (Néelz and Pender, 2010).

Various methodologies have been developed to improve the performance of modelling. These approaches include:

- reduced-complexity models (Liu and Pender, 2010);

- simplified governing equations (Bates et al., 2010);

- parallelisation (Hankin et al., 2008; Neal et al., 2010);

- unstructured mesh (Wang et al., 2010);

- adaptive grid-based methods (Wang and Liang, 2011); and

- grid coarsening (Yu and Lane, 2006a).

Among these methods, unstructured mesh can effectively reduce the computing load and potentially enable more efficient description of surface features, however the pre-processing of terrain data is complex, especially in urban environment (the use of unstructured mesh is beyond the scope of this paper).

On the other hand, grid coarsening appears to be the simplest approach and straightforward for modelling. However, the loss of information with low resolution often leads to less accurate modelling results. The efforts to rectify this problem and to regain some information have included the use of: (1) sub-grid treatment (Yu and Lane, 2006b; Yu and Lane, 2011), (2) porosity parameters (McMillan and Brasington, 2007), (3) multi-cell information from pre-simulations (DHI Software, 2010), (4) progressive morphological filtering of raw LiDAR data (Abdullah et al., 2012).

In urban environment, buildings occupy considerable space and their walls usually exclude deluges from the interior spaces during flooding. The water flows around buildings rather than into or through them, unless their entrances are left open. To characterise the physical situation in overland flow modelling, using the roof elevations (whose resolution is less than

the building scale) in fine grids, is the simplest but computationally costly solution. When the grid size is an order of magnitude greater than the building scale, the ground elevation is commonly used along with *increased local roughness* for numerical simulations. However, such an increase in roughness often has no objective setting criteria to follow. An alternative solution is to take the average elevation of fine cells within a coarse cell as the averaged grid for modelling. Nevertheless, the results are often too coarse to describe the local phenomena often required in practical applications.

To improve the situation with coarse grid modelling, the Building Coverage Ratio (BCR) and Conveyance Reduction Factor (CRF) were introduced to the 2D Urban Inundation Model (UIM) to capture the building features *within* a coarse grid (Chen et al., 2008; Chen et al., 2012). The application demonstrated that the use of BCR and CRFs provide good accuracy of modelling results with considerably smaller computational time. However, it also indicated that the approach failed to reflect the flow phenomena when a building *bisects* a coarse cell. To overcome that problem, in this paper, we developed the *multi-layered approach* and implemented it in the UIM to improve the accuracy of coarse grid modelling with limited extra computational cost. The rest of the paper is organised as follows. The Methodology section explains the details of the multi-layered flood modelling. The Applications and Discussion section compares case studies using different grid coarsening approaches to the benchmark of fine grid modelling. The main findings of the study are described in the Conclusions.

Methodology

The 2D non-inertia UIM, based on the de Saint Venant equations, is adopted in the study for simulating the overland flow propagation on alluvial plains with mild natural topography. The parameters BCR and CRFs are applied to describe building attributes in coarse grid that allow the applications to have accuracy similar to that of the fine grid modelling. The BCR

coefficient, $\alpha = A_b / A$ [-], represents the area ratio occupied by buildings within a computational cell, where A_b is the building area [m²] and A is the grid cell area [m²]. The CRFs, β_x and β_y, as shown in Figure 1, are the maximum occupancy ratios of buildings on the computational cell *boundaries* in the x and y directions, respectively, that flow cannot transfer through. The governing flow equations modified to account for CRFs are expressed as follows:

$$(1 - \alpha) \frac{\partial d}{\partial t} + \frac{\partial \left[(1 - \beta_x) u d \right]}{\partial x} + \frac{\partial \left[(1 - \beta_y) v d \right]}{\partial y} = q \tag{1}$$

$$\frac{\partial (d + z)}{\partial x} + \frac{n^2 u \sqrt{u^2 + v^2}}{d^{4/3}} = 0 \tag{2}$$

$$\frac{\partial (d + z)}{\partial y} + \frac{n^2 v \sqrt{u^2 + v^2}}{d^{4/3}} = 0 \tag{3}$$

where, (1) is the continuity equation and (2)-(3) are the momentum equations in the horizontal Cartesian directions; d is the water depth [m]; u and v are the velocity components in the x and y directions, respectively [m/s]; z is the surface elevation [m]; n is the Manning roughness coefficient; q is the rate of water entering or leaving ground surface per unit area, comprising the excess rainfall, the upstream catchments inflows, the influent and effluent of sewer network nodes within a cell, and any overland flow drained by hydraulic facilities [m/s].

Details about the methodology of UIM with BCR & CRFs were discussed in a separate paper (Chen et al., 2012). The coupled BCR & CRFs enabled a representation of the available storage space within a coarse grid cell and the effective conveyance width between neighbouring cells. The modelling results showed that – rather than changing grid roughness by trial and error – this approach provided an objective way, to reflect the blockage effect induced by buildings using coarse grid modelling. Nevertheless, the BCR &

CRFs approach had failed to describe the regime that flow was diverted or blocked by buildings that *bisect* a coarse cell (to be explained in next paragraph). To deal with the situation, we propose the multi-layered approach to divide the potential storage area into separate regions for modelling. In contrast, the previous BCR & CRFs approach (Chen et al., 2012) is referred as the single layer approach in the following text.

Figure 2 shows two simple examples for BCR & CRFs applications. The channels in both Figure 2-(a) and Figure 2-(b) have a width of 4 and a length of 12 fine grid cells (or a width of 1 and a length of 3 coarse grid cells), with the northern and southern boundaries closed, and the eastern and western boundaries open. The building in Figure 2-(a) is located at the four fine cells in the centre of a coarse cell, whereas the one in Figure 2-(b) occupies the four cells that completely disconnect the domain into two parts. The inflow applied to the western boundary traverses the channel in Figure 2-(a) but is blocked in Figure 2-(b). The single layer approach generates the same BCR & CRF values for both layouts, causing the building influence on surface flow identical in modelling. This misrepresentation of the building layout would result in no outflow at the eastern boundary in Figure 2-(b). If the domain in Figure 2-(b) is extended both northwards and southwards in coarse grid modelling, as shown in Figure 3-(a), the flows from the west to the central coarse cell in the fine grid modelling is separated into two routes to reach the cell in the east. The BCR & CRFs in the single-layer approach cannot describe the separation of flow such that the coarse grid modelling will allow the flow to propagate through the central cell from west to east without any obstruction. Figure 3-(b) shows that the six possible flow paths between the central cell and its four neighbours.

In order to describe the flow interactions comprehensively in the multi-layer approach, the central cell in Figure 4-(a) is considered as the combination of two layers (Layer 0 and 1) of cells as shown in Figure 4-(b) and (c). Both cells reflect the different attributes of the areas

that are bisected by the building within the coarse cell. Figure 4-(b) shows that the Layer 0 central cell has a BCR value 0.5, which means only 50% of cell area is available for flood storage in the west region of the coarse cell. The CRF values at the west, north and south cell boundaries are 0.0, 0.5 and 0.5, respectively, which allows water movement between the Layer 0 central cell and the three neighbour cells via paths P1-P3, as shown in Figure 5-(a). The CRF value at the east boundary is 1.0, which prevents the flow movement from any of the three boundaries to the east.

On the contrast, Figure 4-(c) shows the Layer 1 central cell has a BCR value 0.75, which represents that only 25% of coarse cell area is available for flood storage in the east region. The CRF values at the north, south and east cell boundaries are 0.75, 0.75 and 0.0, respectively, which allows the water movements between the Layer 1 central cell and the neighbour cells via paths P4-P6, as shown in Figure 5-(b). The CRF value at the west boundary is 1.0, which prevents the flow movement from any of the three boundaries to the west.

Figure 5-(c) is the schematic presentation for the relationships between the coarse cells. The central cell is divided into two smaller cells with reduced storage areas. For each time step calculation, the momentum equations along flow paths between all Layer 0 cells over the whole domain are firstly solved using the original UIM routine. Then, the momentum equations along flow paths between Layer 0 cells and the Layer 1 central cell are solved where such flow paths exist. In case of more than two layers (such as in the two case studies discussed later), corresponding momentum equations would need to be solved in a similar manner. Finally, the continuity equations are solved in the same sequence. Since the two central cells (Layer 0 and 1) are treated separately, the flow interaction between them is not permitted, which represents correctly the physical phenomenon that flow between the two regions is blocked by the building.

The described principles for setting up the Multilayer parameters are simple. Nevertheless, the calculations of the BCR & CRFs, the level of Multilayers and the linkages between cells of different layers become complex if more than two layers are required. An appropriate post-processing is also required to remap the modelling results back to correct positions on the fine grid. All this would be a demanding task in large areas with thousands of buildings. We adopted a cellular automata (CA) approach to flag out all coarse cells bisected by buildings, and calculate automatically all the relevant parameters. The CA model searches all non-building fine cells within a coarse cell to identify consecutive non-building areas. Each identified area is indexed as a coarse cell layer and its BCR is calculated. Then, the flow paths between neighbour coarse cell layers and the corresponding CRFs are determined. Evans et al. (2009) proposed the original methodology of the CA model that can generate BCR and CRFs for the single layer approach. The advanced version (Evans et al., 2012) has been extended to the multi-layered approach and applied to the examples shown in this paper.

Applications and discussion

Synthetic case study

The first case study was selected to be an E-shaped building on a 400m x 100m 'ski run' surface, following the previous single layer BCR & CRFs application (Evans, 2010). The arrangement of the building was complex enough to demonstrate the difference between single layer and multi-layered approaches. The terrain consisted of three sections, as shown
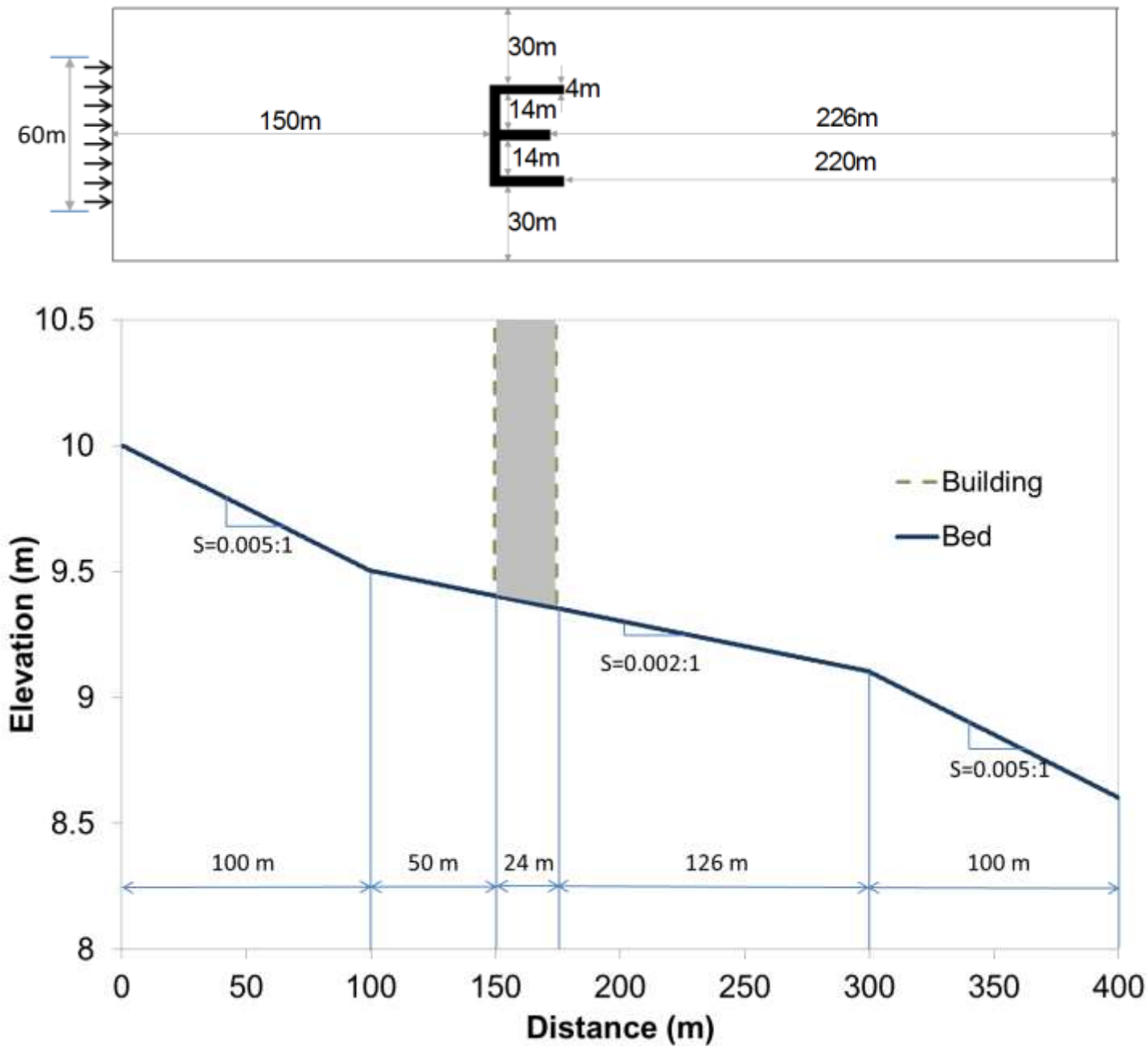
in

Figure 6, the first and the last 100m sections had a slope 0.005:1 (V:H) and the middle 200m section had a milder slope 0.002:1. The northern and southern boundaries were closed and the eastern boundary was open. A lateral discharge, shown in Figure 7, was introduced at the western boundary and distributed uniformly over a 60m central swath (30m either side of the centre line bisecting the x-axis where y = 0). The normal flow depth was set as the downstream condition at the eastern boundary. These boundary conditions were applied to

ensure the propagation of flow along the surface from west to east. The E-shaped building with 4m height was located in the middle section of the domain and the building's orientation was such that its closed face was perpendicular to the incoming surface flow.

Three coarsening approaches (averaged DEM, single layer and multi-layered) with 20m grid resolution were compared to the benchmark. The benchmark was assumed to be the simulation on a fine 1m grid with terrain elevations that include building heights, with buildings positioned such that each fine grid cell is either fully or not at all covered by a building. The averaged DEM took the mean of ground and roof elevations of fine cells within a coarse cell as the new elevation of the coarse cell. The single layer approach adopted the mean of the ground elevations of fine cells that were not occupied by buildings to represent the new elevation of a coarse cell, with the calculated BCR & CRFs. The multi-layered approach determined the new ground elevation of each layer based on the average elevation of non-building fine cells in the layer. The individual BCR & CRFs were calculated for the extra layers and flow paths.

Figure 8 shows the layer index and BCR values of Layer 0 of the coarse cells surrounding the E-shape building. The overall layout around the building feature can be shown as the schematic map shown in Figure 9. The circle size represents the available storage area, the arrows represent the flow path between cells in multiple layers, the value associated with each arrow represents the CRF value and the colour represents the corresponding layer number as shown in Figure 8. The preservation of the building features in the 20m resolution was achieved by using additional 6 grid cells and 10 pathways connecting them accordingly, which is 7 pathways more than in a single-layer approach.

The error distribution maps of the coarse grid modelling results, as compared to the fine-grid benchmark, are shown in Figure 10. The averaging with building roof height raised the terrain elevation that expanded the building areas in the coarse grid. For the 20m resolution,

the widths of flow paths on north and south sides of building were reduced from 30m to 20m each due to the over-estimated building areas, which resulted in significant blockage effect on the upstream side of the building, as shown in Figure 10-(a). The errors of the single layer approach in Figure 10-(b) show that the BCR & CRFs did not describe the layout where the building bisected coarse cells.

The reasons for this are illustrated in

(a)   (b)

Figure 11-(a), which shows the original building alignment within 20m resolution grid in the single layer approach.

(a)   (b)

Figure 11-(b) is a similar setting but with gaps between buildings, and the compensation building areas were added back to have equivalent BCR values in

(a)   (b)

Figure 11-(a). Although the widths of flow paths on cell interfaces where the 4m building walls occupied were reduced by 20% in

(a)   (b)

Figure 11-(a), the approach did not prevent the flow interactions between both sides of the building and both settings in

(a)   (b)

Figure 11-(a) and (b) had identical flow behaviour, i.e. the single layer approach cannot distinguish between these two cases. Therefore, the water transferred from the west side of the building directly into the inner area resulted in a large underestimation error on the upstream side of the building and an overestimation on the downstream side. Because the flow in the multiple layer modelling was blocked by the building completely instead of having width reduced flow paths, the backwater effect increased on the upstream side of the building with less overestimation of flood depths on the downstream side than in the single layer case, as shown in Figure 10-(c).

Figure 12 shows the maximum flood depth profiles along the central line in the x direction of different modelling results. The profile of the multi-layered approach is clearly much closer to the benchmark model than other two approaches. As no flow is allowed through the building using this method the maximum depth errors after the building are thus significantly reduced when using the multilayer approach.

Table 1 shows the root mean squared error (RMSE) of the calculated maximum flood depths for the three approaches against the benchmark model for the whole computing domain and the middle section, where the building was more influential on the flow movement. These results reveal that the multi-layered approach offered a significant improvement over the averaged DEM and the single layer approaches.

Table 2 shows that the model efficiency of the multi-layer approach is good, i.e., the reduction of the number of grid cells greatly reduces the computing time for coarse grid modelling. As the multi-layered model requires more computing time for solving those extra layers and flow paths, and remapping the coarse data back to the fine grid at selected output timing, the overall running time was only slightly longer than the other two grid coarsening approaches. Nevertheless, the multi-layered modelling, with the added advantage of maintaining building integrity and subsequent flow-path routing, is more accurate such that the minor additional time required is negligible when assessing the model performance.

Real case study

In the following example a 300m x 300m LiDAR tile at a 1m resolution shown in Figure 13 was applied to test the multiple-layered approach in real urban environment. This surface model was coarsened using above-mentioned three methods to a 12m resolution. Rainfall was introduced directly onto the 2D surface flow model over the whole region and – in case of the multi-layered approach – into each layer simultaneously. It was assumed that any rainfall that lands upon a building roof will be drained directly to a sewer and therefore will

not move across the surface, hence the rainfall was only applied to the surface regions where there are no buildings present. For this particular simulation the duration of the input rainfall was one hour and was applied at a constant intensity 60mm/h. The overall simulation time was 90 minutes which allowed a 30-minute period for water movement across the surface after the rainfall has stopped.

Figure 14 shows the maximum flood depth distribution on the 1m resolution benchmark and the three coarse grid models. The pattern of water distribution reveals three areas with significant ponding of surface water, which are highlighted as regions A, B and C. The benchmark result, Figure 14-(a), shows that water accumulated in region A and then flew through the narrow alleyway in the east section of the terrace on the north side of region A to location of region B. The water in this region then propagated via two alleyways between buildings to the street on the north side of the terrace that connects to region C. When the built-up water depths in region B were large enough, the flow path around the south side of the building next to the north-east boundary of region B was formed that allowed the surface water to move towards region C.

Figure 14-(b) shows the averaged DEM approach not only led to the loss of alleyways between buildings, it also caused the narrowing of street channels that convey surface water. No flow path via narrow alleyways between buildings was formed such that more water (with greater flood depths) ponded in the north-western, the south-eastern and the south-western upstream areas. Less flooding occurred in the downstream areas, especially region C. Meanwhile, the assumption was that rainfall falling on building roof was drained to sewer system directly. In the averaged DEM approach, a cell is normally regarded as a non-building cell unless it is completely occupied by buildings, such that the surface runoff can flow to neighbour non-building cells quickly because of the significant difference of elevations. Therefore, same flood depth covers the whole coarse cell area even though it is

partially occupied by buildings. Meanwhile, pre-processing to multiply the rainfall amount by the non-building coverage area ratio of a cell was required to determine the rainfall input to each cell.

Figure 14-(c) shows that the single layer approach produced closer modelling result than the averaged DEM one to the benchmark. The flood depth only represents the flow condition of non-building area within a coarse cell. However, it also yielded a significant underestimation in surface depths within region A as a result of further erroneous (with respect to benchmark model) flow routing through previously obstructed alleyways (to be discussed later). Similar situation occurred for the water moving from region B to downstream region C. The water transferred from region B to the street on the north directly such that the flow path around the south side of the building next to region B was not formed. This resulted in greater flood depths and extent than other two grid coarsening approaches in region C.

Figure 14-(d) shows that the multi-layered approach had by far closest modelling result to the benchmark model. Multiple flood depths within a coarse cell are obtained for all separated non-building areas. The alleyway in the east section of the buildings on the north side of region A allowed the flow propagating from region A to region B. The water in region B further flew to the street on the north side via the alleyways between buildings, as well as bypassing the south side of the building next to region B. The representations of buildings and the patterns of flow movements were better described in the multi-layered approach than in the other two grid coarsening approaches.

Figure 15-(a) shows the detailed maximum flood depths near the alleyways in the west section of the buildings (the outlined area next to region A in Figure 14) on the north side of region A. Three alleyways with widths less than 1m were represented as blocked in the benchmark model due to the resolution of terrain data.

In the coarse grid modelling, the representations of the two cells highlighted in Figure 15-(b), 15-(c) and 15-(d) resulted in significant differences of results. In the averaged DEM approach, as shown in Figure 15-(b), the alleyways between buildings were completely lost, as discussed above, and the whole section was modelled as single terraced house.

In the single layer approach, as shown in Figure 15-(c), the flow was allowed to move from one cell boundary to any other boundary of the highlighted cells because neither side had CRF=1 and the internal blockage was not considered.

In the multi-layered approach, as shown in Figure 15-(d), the non-building areas of the top-right highlighted cell was divided into five layers for modelling. The setting prevented the flow transferring from the south and the east sides to the north and west sides. The bottom-left highlighted cell was modelled as two layers and the flow interactions among the north, east and south sides were possible in the same layer. Nevertheless, the layer of its north neighbour cell can only interact with the highlighted cell such that the flow movement via the alleyway was also blocked, which was the same as in the benchmark model.

Figure 16 shows the detailed maximum flood depth in the region B, which is outlined in Figure 14. In the benchmark model, as mentioned earlier and shown in Figure 16-(a), the surface water left region B either via the two alleyways in the west section of buildings on the north or bypassing the south side of the building on the east.

Figure 16-(b) shows that the averaged DEM approach completely stopped the flow interaction between region B and the street on the north, therefore, less flooding occurred along the street.

In the single layer approach, as shown in Figure 16-(c), the flow was allowed to move across the highlighted cells from region B to the street on the north. Therefore, simulated flood depths in region B were smaller.

For the multi-layered approach, as shown in Figure 16-(d), the two alleyways affected modelling results in the same manner as in the benchmark. Each of the two highlighted cells were modelled as two separated layers that forbid the direct flow interaction between region B and street on the north. More water was trapped in region B and then the flow path bypassing the south side of the building was formed. Consequently, the overall modelling result was much similar to the benchmark one.

Although three alleyways shown in Figure 15 were blocked in the benchmark model, it is clear that the modelling result may not be correct because they were not properly described in the terrain data. The alleyways narrower than the resolution of terrain data are likely to be blocked, especially when their orientation is not parallel/orthogonal to the grid axes. Further study to clear up such alleyways from the terrain data would be necessary to provide better modelling.

Conclusions

The originally developed multi-layered approach to regular grid 2D urban flood modelling has been presented in this paper. Through implementation of BCR and CRF coefficients and the accordingly modified flow equations, this method enables computation of flows separated by buildings within a coarse grid cell. Automatic generation of layers and calculation of BCR and CRFs using a cellular automata based flagging has been implemented and tested in conjunction with the modified UIM model.

Through the comparisons on two case studies (a synthetic and a real one), it has been shown that the multi-layered approach gives results much closer to a high-resolution benchmark than the single layer model (whilst the latter is in turn much more accurate than the simple DEM-averaging approach). The increased accuracy of the multi-layered approach comes at only insignificantly increased computational cost. Therefore, this approach lends itself for 2D modelling on a coarse grid with a good balance between

accuracy and computational speed. In practical applications, a desired (or "optimal") choice of the coarse grid size can easily be identified through error analysis in numerical experiments similar to those presented in this paper.

The implementation of the multi-layered approach in conjunction with any other raster grid based 2D model would require a modification of flow equations to include additional layers and CFRs, however that is fairly straightforward. Without the modifications of other authors' models – i.e. on the basis of our research alone – it is not possible to conclude if and to what extent the multi-layered approach is superior to known improvements of coarse grid modelling mentioned in the introduction. However, it is anticipated that the improvement offered by our approach may be at least as good as sub-grid treatment, porosity parameters or multi-cell information. This expectation – that is yet to be checked – is based on the fact that multi-layered model is very flexible due to efficient automatic generation of layers and calculation of BCR & CRFs, and it is realistic in the sense that it explicitly treats pathways separated by buildings within a grid cell.

In conclusion, with the introduction of multiple layers, the possibility of a much faster 2D surface flow modelling on a coarse grid – with nearly a fine-grid accuracy – can be efficiently achieved. In other words, larger scale urban inundation can be simulated within time that a high resolution model would require on a much smaller limited extent of urban area.

The real case study results highlighted, however, that some narrow alleyways not represented properly due to LiDAR data resolution need additional attention in modelling. Potentially, the problem can be solved if higher resolution of terrain data is made available. However, the multi-layered approach can extract key features and model the detailed flow movement even without using finer grid resolution, which would require creation of pathways and CRFs different from the one described in this paper. In real urban environment, infrastructure such as flyovers, underground passages, bridges, etc., also alters the

propagation of surface runoff. The multi-layered methodology can be efficiently used to describe multiple flow paths that cross over each other within a cell such that the complex flood propagation phenomena can be modelled.

Acknowledgements

References

Abdullah, A.F., Vojinovic, Z., Price, R.K., Aziz, N.A.A., 2012. A methodology for processing raw LiDAR data to support urban flood modelling framework. J Hydroinform, 14(1): 75-92.

Bates, P.D., Horritt, M.S., Fewtrell, T.J., 2010. A simple inertial formulation of the shallow water equations for efficient two-dimensional flood inundation modelling. Journal of Hydrology, 387(1-2): 33-45.

Chen, A.S., Djordjević, S., Leandro, J., Evans, B., Savić, D., 2008. Simulation of the building blockage effect in urban flood modelling, 11th International Conference on Urban Drainage, Edinburgh, Scotland, UK.

Chen, A.S., Evans, B., Djordjević, S., Savić, D.A., 2012. A coarse-grid approach to representing building blockage effects in 2D urban flood modelling. Journal of Hydrology, 426: 1-16.

DHI Software, 2010. MIKE 21 FLOW MODEL Hydrodynamic Module Scientific Documentation, DHI Software, Hørsholm, Denmark.

Environment Agency, 2009. Flood and coastal risk management in England: A long-term investment strategy, Environment Agency.

Evans, B., 2010. A multilayered approach to two-dimensional urban flood modelling, University of Exeter, Exeter, United Kingdom.

Evans, B., Chen, A.S., Djordjević, S., Savić, D.A., 2009. A Cellular Automata based approach to Generalising Digital Terrain Models for 2D flood modelling, 8th International Conference on Urban Drainage Modelling, Tokyo.

Evans, B., Chen, A.S., Djordjević, S., Savić, D.A., 2012. An automated approach to generating multi-layered data for the improvement of two dimensional flood modelling. J Hydroinform, in review.

Hankin, B., Waller, S., Astle, G., Kellagher, R., 2008. Mapping space for water: screening for urban flash flooding. Journal of Flood Risk Management, 1(1): 13-22.

Jenkins, G.J. et al., 2009. UK Climate Projections: Briefing report, Met Office Hadley Centre, Exeter, UK.

Liu, Y., Pender, G., 2010. A new rapid flood inundation model, First IAHR European Congress, Edinburgh, UK.

McMillan, H.K., Brasington, J., 2007. Reduced complexity strategies for modelling urban floodplain inundation. Geomorphology, 90(3-4): 226-243.

Mitchell, J.K., 2003. European river floods in a changing world. Risk Analysis, 23: 567-574.

Neal, J.C., Fewtrell, T.J., Bates, P.D., Wright, N.G., 2010. A comparison of three parallelisation methods for 2D flood inundation models. Environmental Modelling & Software, 25(4): 398-411.

Néelz, S., Pender, G., 2010. Benchmarking of 2D Hydraulic Modelling Packages Heriot Watt University, Edinburgh.

Pitt, M., 2008. The Pitt Review: Lessons learned from the 2007 floods, Cabinet Office, London.

United Nations, 2010. World Urbanization Prospects: the 2009 Revision, United Nations, Department of Economic and Social Affairs, Population Division, New York 2010.

Wang, J.P., Liang, Q., 2011. Testing a new adaptive grid-based shallow flow model for different types of flood simulations. Journal of Flood Risk Management, 4(2): 96-103.

Wang, X., Cao, Z., Pender, G., Neelz, S., 2010. Numerical modelling of flood flows over irregular topography. Proceedings of the Institution of Civil Engineers-Water Management, 163(5): 255-265.

Yu, D., Lane, S.N., 2006a. Urban fluvial flood modelling using a two-dimensional diffusion-wave treatment, part 1: mesh resolution effects. Hydrological Processes, 20(7): 1541-1565.

Yu, D., Lane, S.N., 2006b. Urban fluvial flood modelling using a two-dimensional diffusion-wave treatment, part 2: development of a sub-grid-scale treatment. Hydrological Processes, 20(7): 1567-1583.

Yu, D., Lane, S.N., 2011. Interactions between subgrid-scale resolution, feature representation and grid-scale resolution in flood inundation modelling. Hydrological Processes, 25(1): 36-53.

Table 1. The RMSE for the overall domain and middle section for the synthetic case study for the averaged DEM, the single layer and the multi-layered models against the benchmark

	Averaged DEM	Single layer	Multi-layered
Overall domain RMSE (mm)	38.2	15.0	6.0
Middle section RMSE (mm)	53.0	20.6	5.7

Table 2. Model properties and computing time of the synthetic case study for the benchmark, the averaged DEM, the single layer and the multi-layered models

	Benchmark	Averaged DEM	Single layer	Multi-layered
Grid resolution	1m	20m	20m	20m
No of cells	40,000	100	100	106
Computing time	27,004s	2.4s	1.2s	2.7s
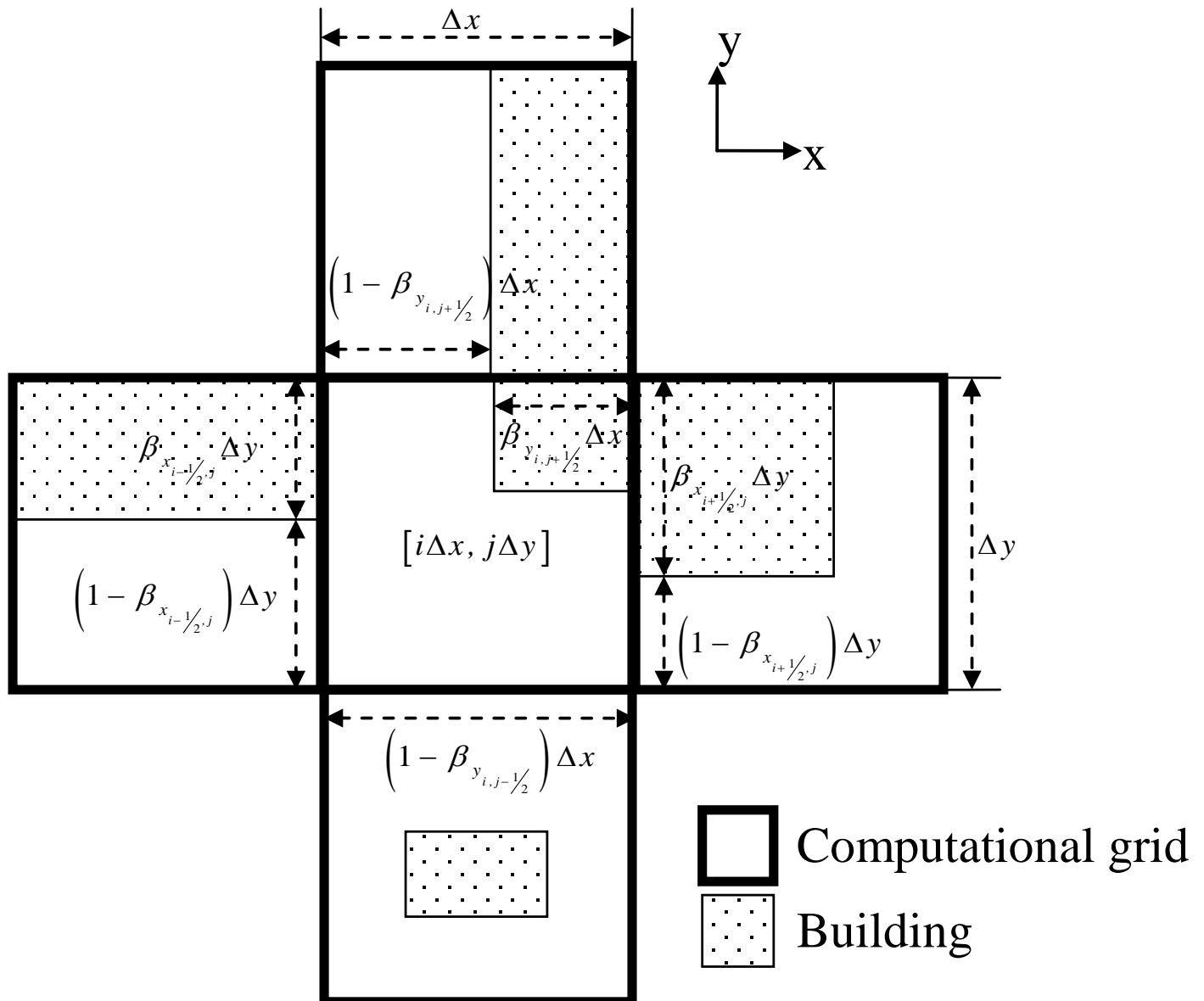
Figure 1. The determination of the CRFs for a computational grid based on the building alignments within itself and its neighbourhood grids at cell boundaries.
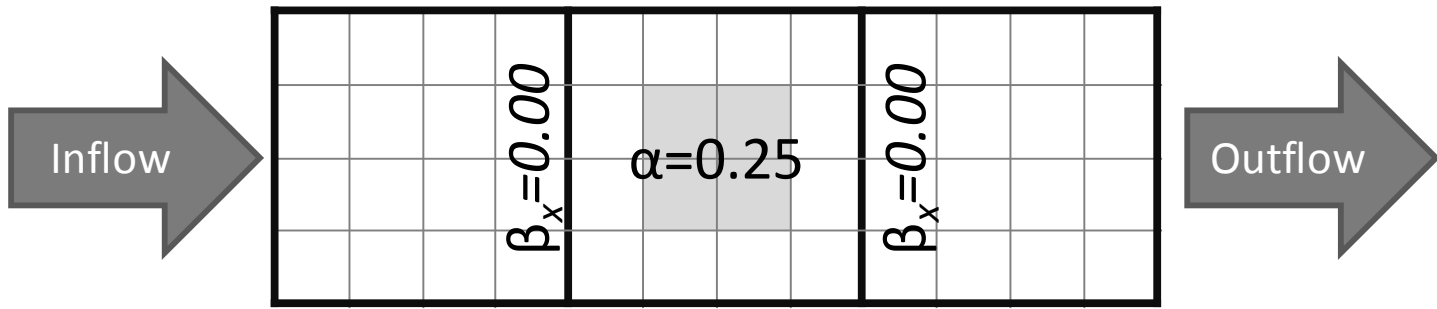
(a)
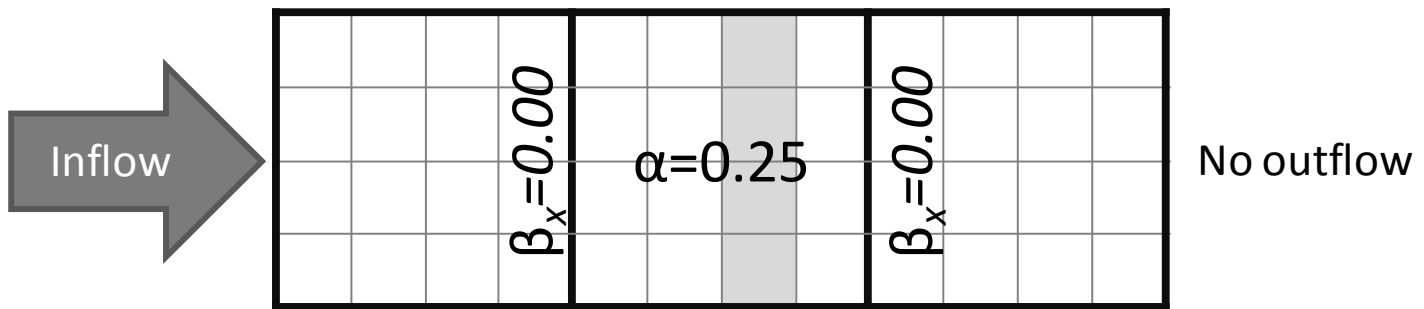
(b)

Fine empty cell   Fine building cell   Coarse cell

Figure 2. Different building layouts within a coarse cell result in same BCR and CRFx values

(a)

(b)
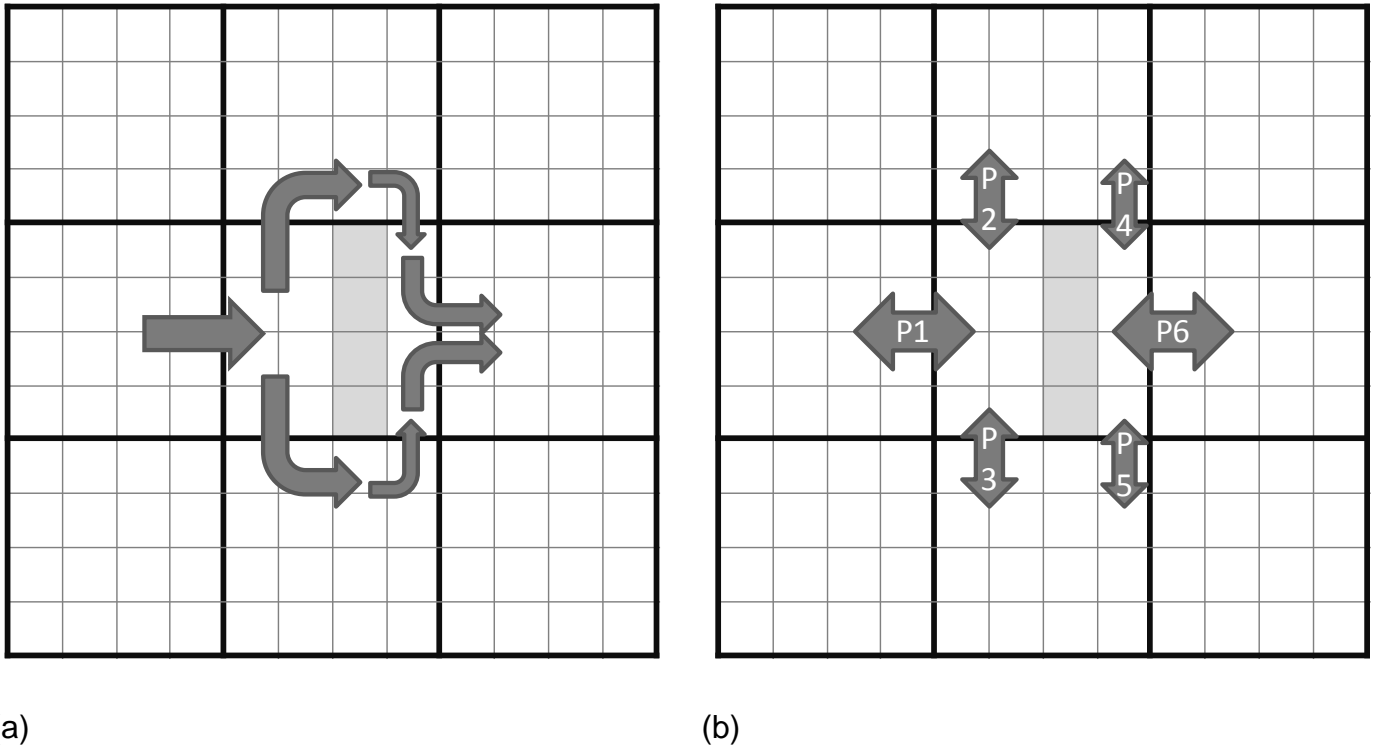
Figure 3. (a) Flow from the west moves around the building that bisects a coarse cell to reach the east. (b) Six possible flow paths between the central cell with its neighbour cells.
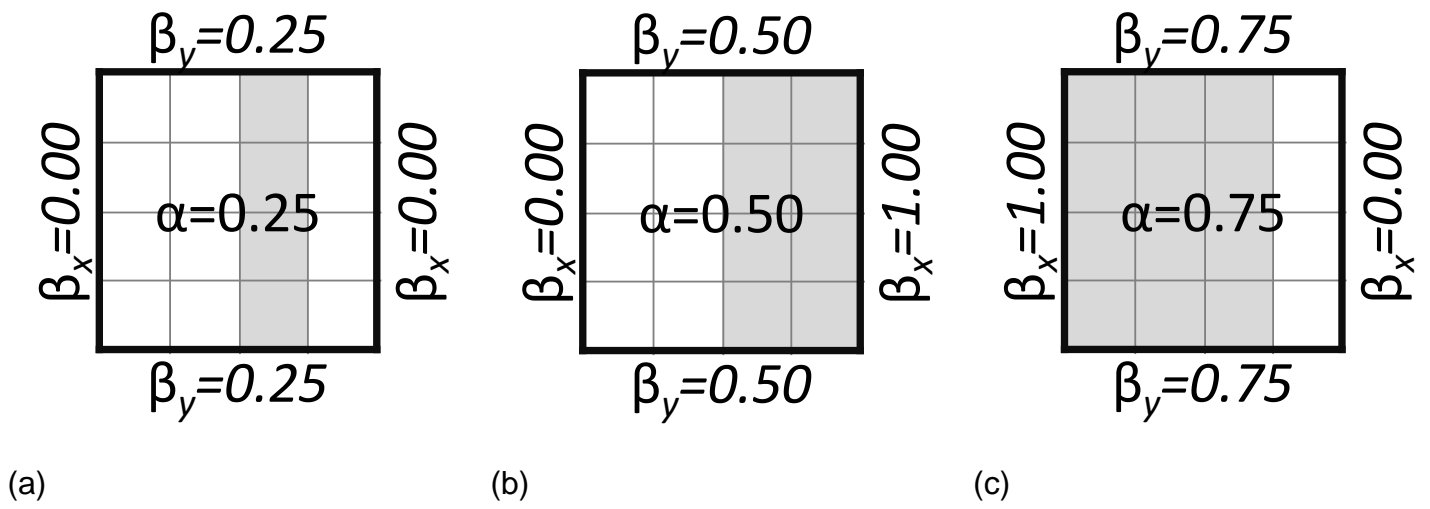
Figure 4. (a) The central coarse cell in Figure 3 is represented by the multi-layered cells of (b) Layer 0 and (c) Layer 1

(a)   (b)   (c)
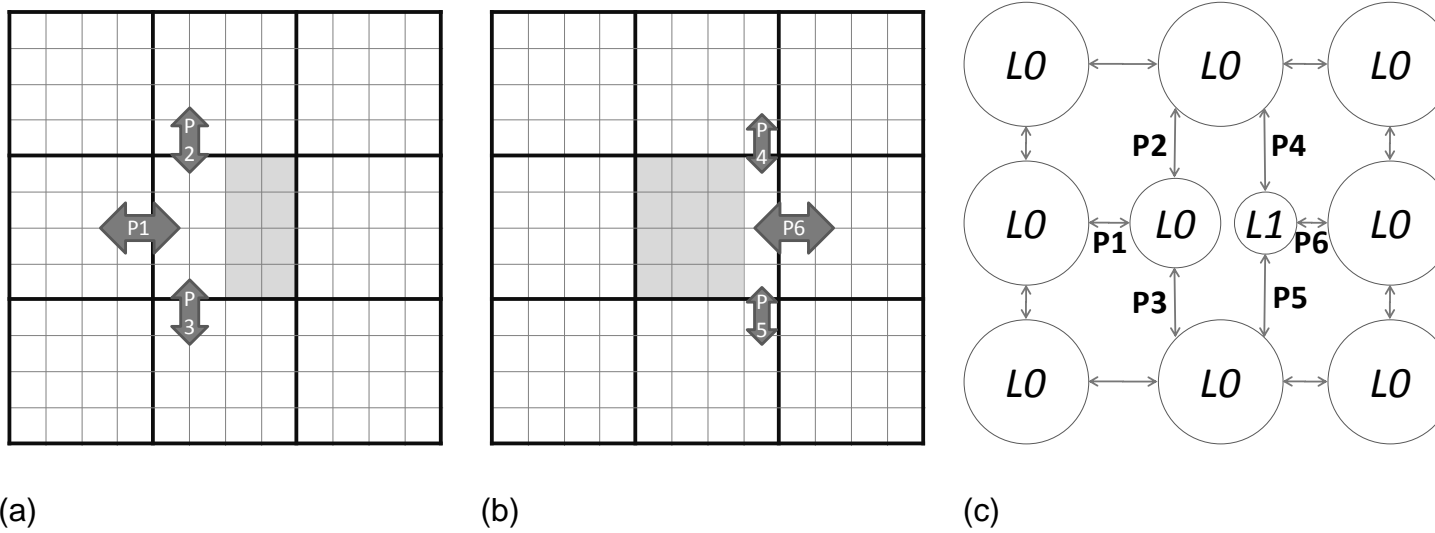
Figure 5. (a) The Layer 0 central cell used for describing the flow paths between the central cell and its west, north and south neighbour cells. (b) The Layer 1 central cell used for describing the flow paths between the central cell and its north, south and east neighbour cells.
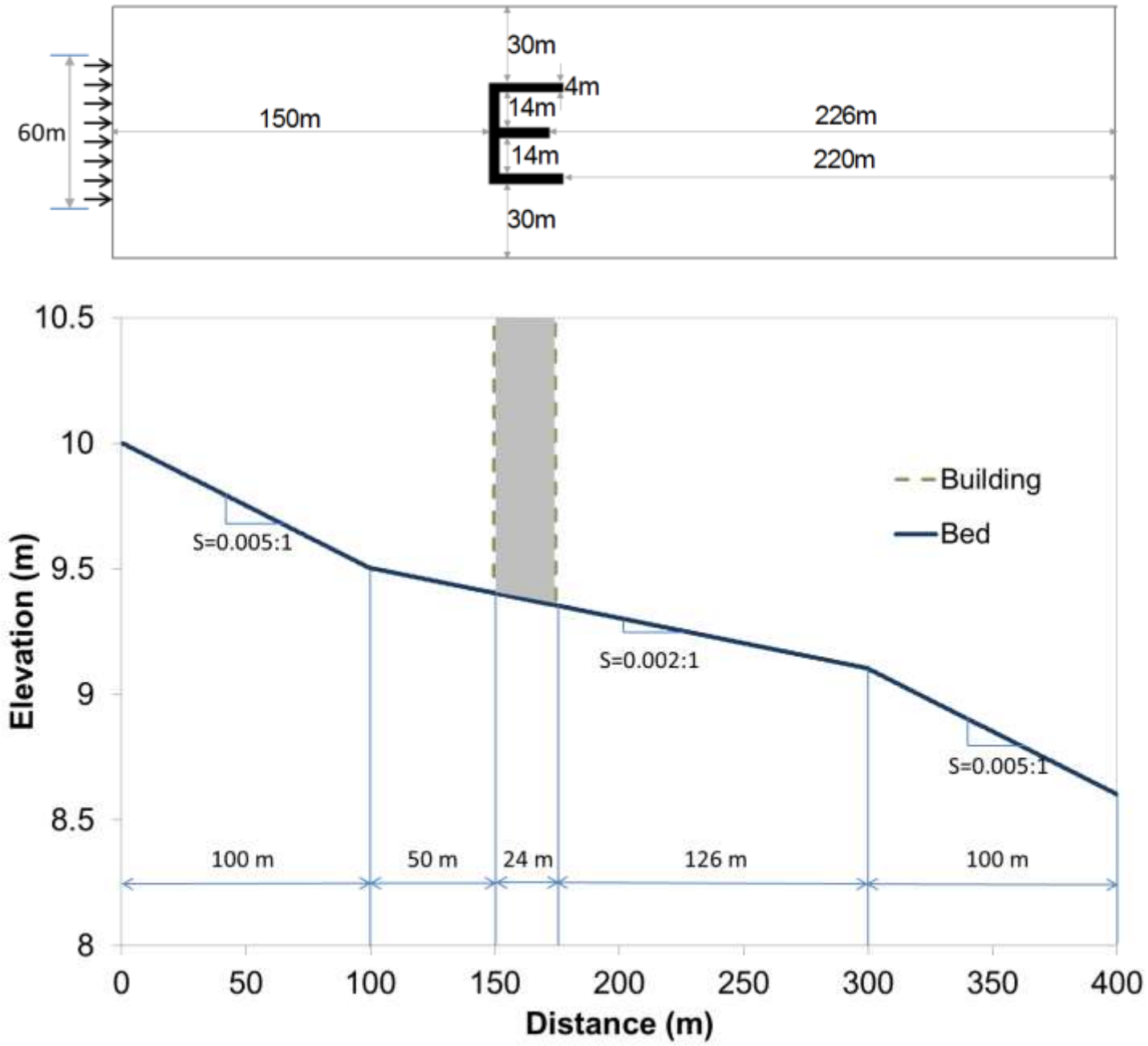
Figure 6. The plain view (up) and the longitudinal elevation profile (down) along the central line of the 2D case study.
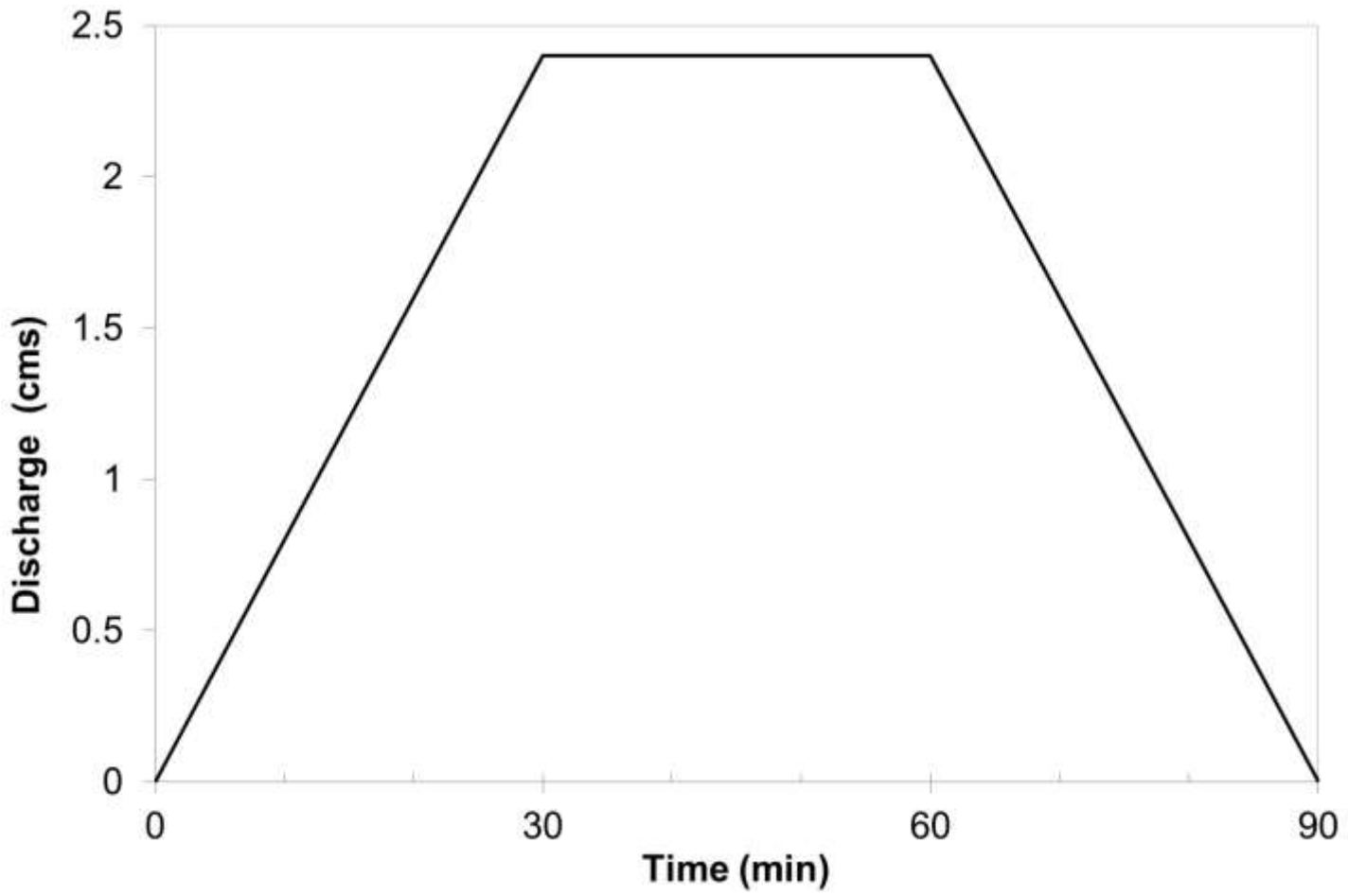
Figure 7. Lateral flow input at x=0
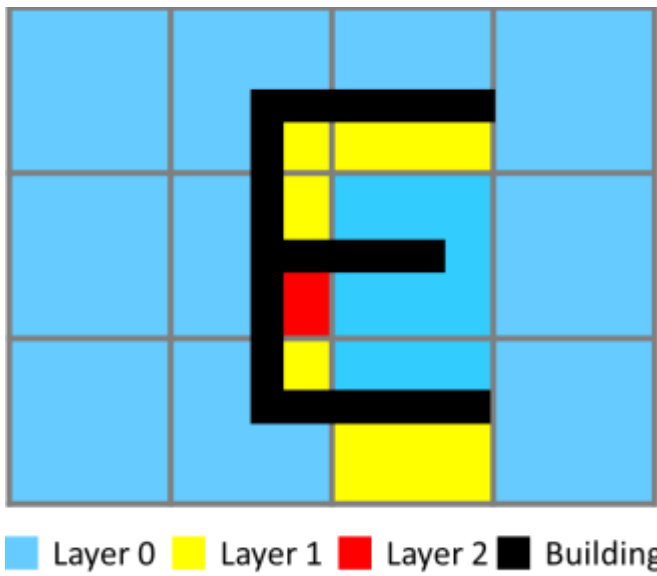
(a)   (b)

Figure 8. Grid plain view of (a) multiple layers and (b) BCR for Layer 0 using the multi-layered approach
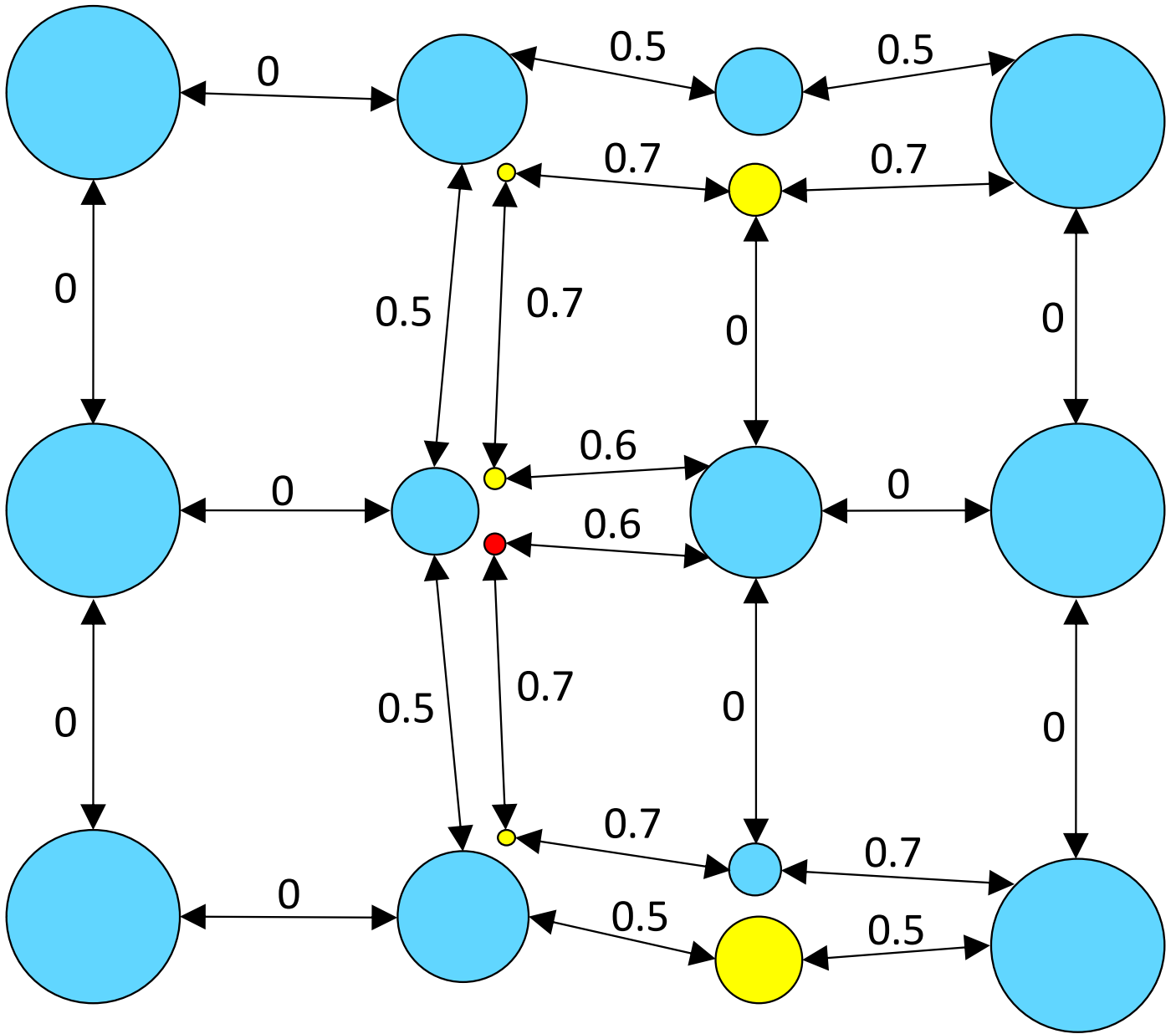
Figure 9. Multi-layered concept map of the section shown in Figure 8

(a) Averaged DEM

(b) Single layer

Error (m)

	-0.0914 - -0.05
	-0.0499 - -0.02
	-0.0199 - -0.01
	-0.0099 - -0.001
	-0.0009 - 0.001
	0.0011 - 0.01
	0.0101 - 0.02
	0.0201 - 0.05
	0.0501 - 0.1
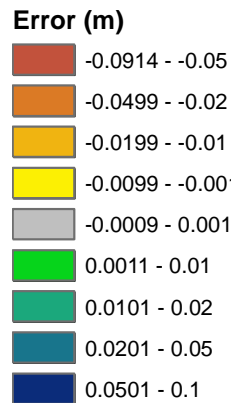
(c) Multi-layered

Figure 10. The distribution of the errors of maximum flood depths for simulations of (a) the averaged DEM (b) the single layer and (c) the multi-layered approaches

(a)   (b)
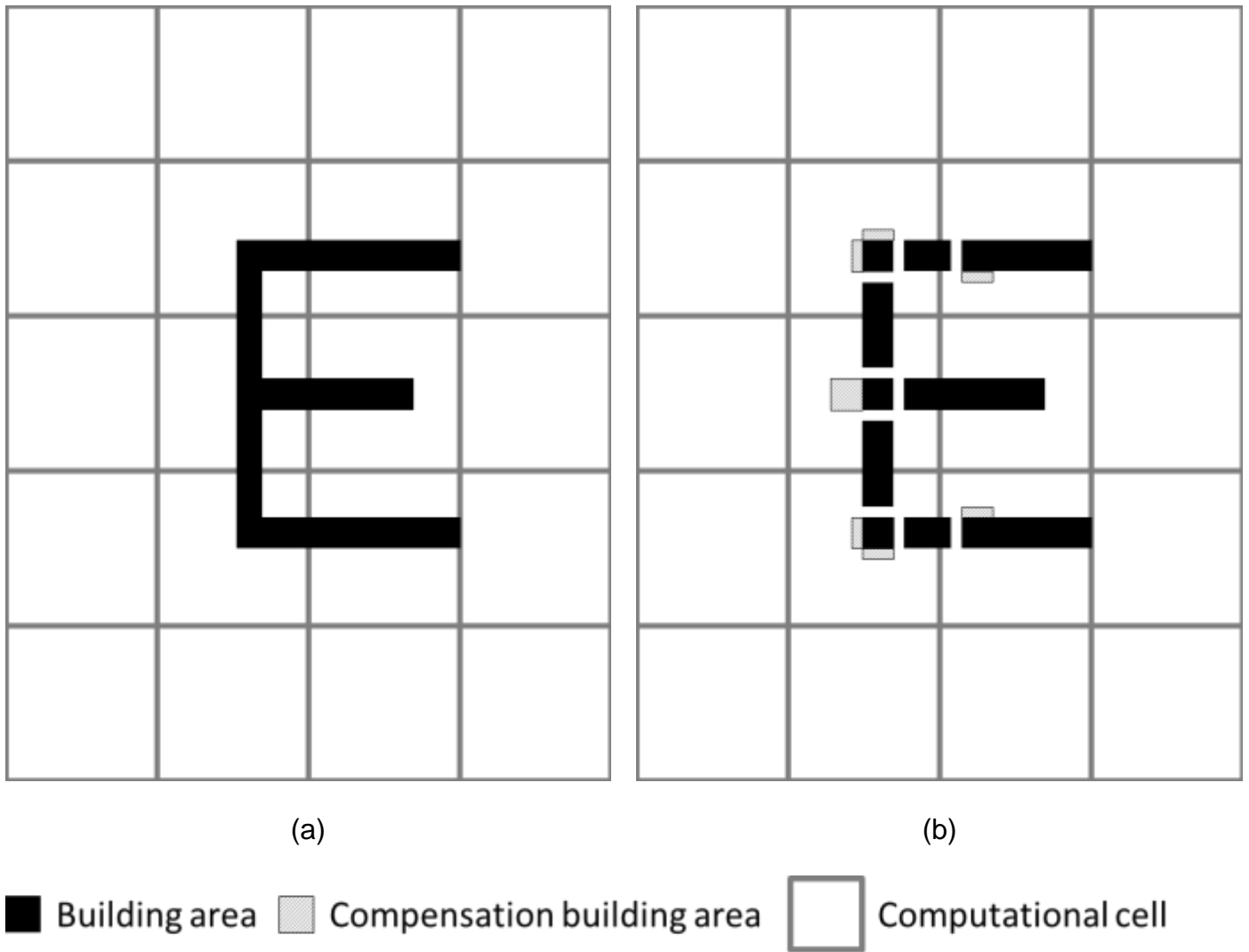
Figure 11. The E building alignment within 20m resolution grid (a) original setting (b) equivalent setting with gaps between buildings
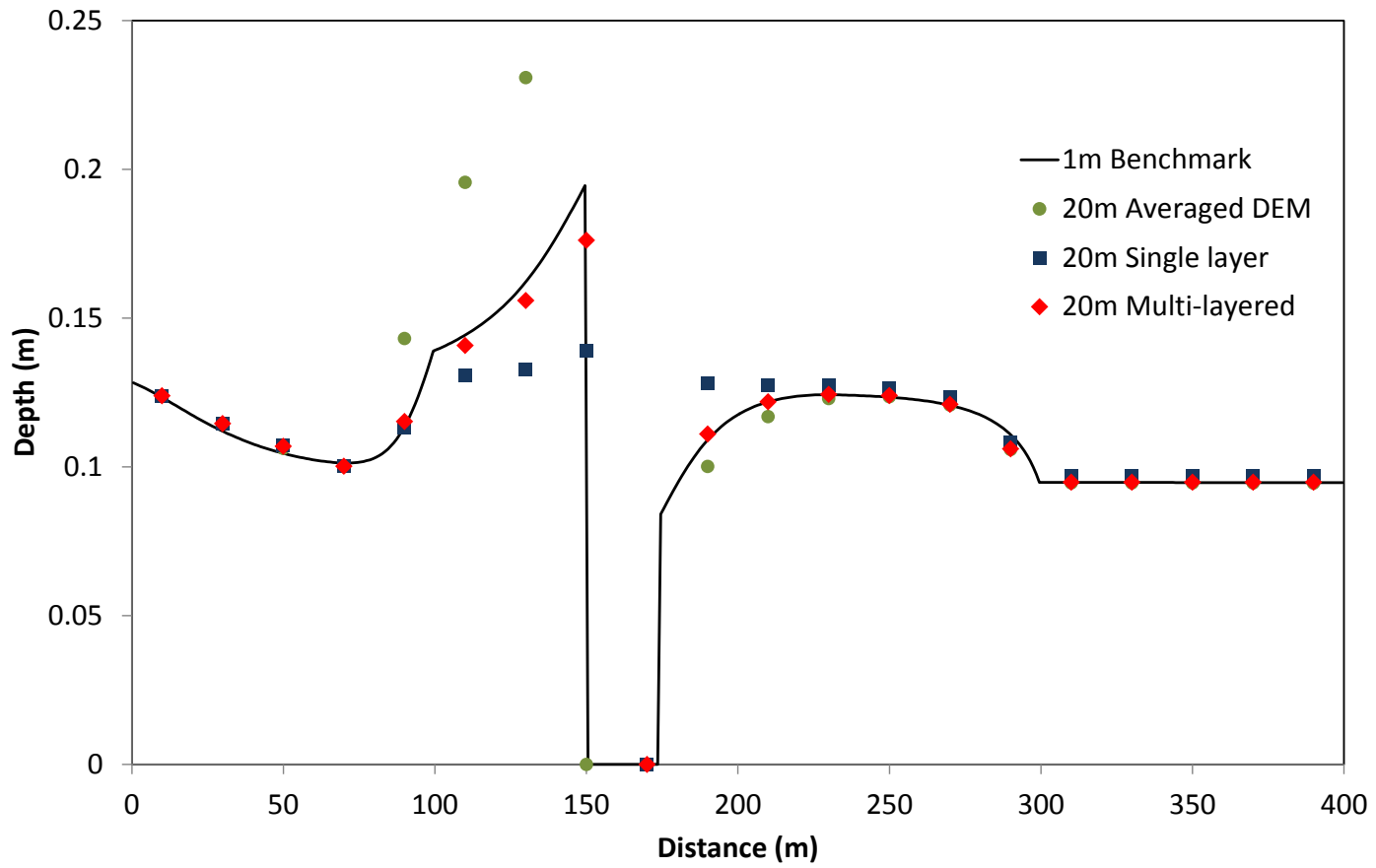
Figure 12. The comparison of flow depths along the central line of the averaged DEM, the single layer and the multi-layered models with the benchmark model
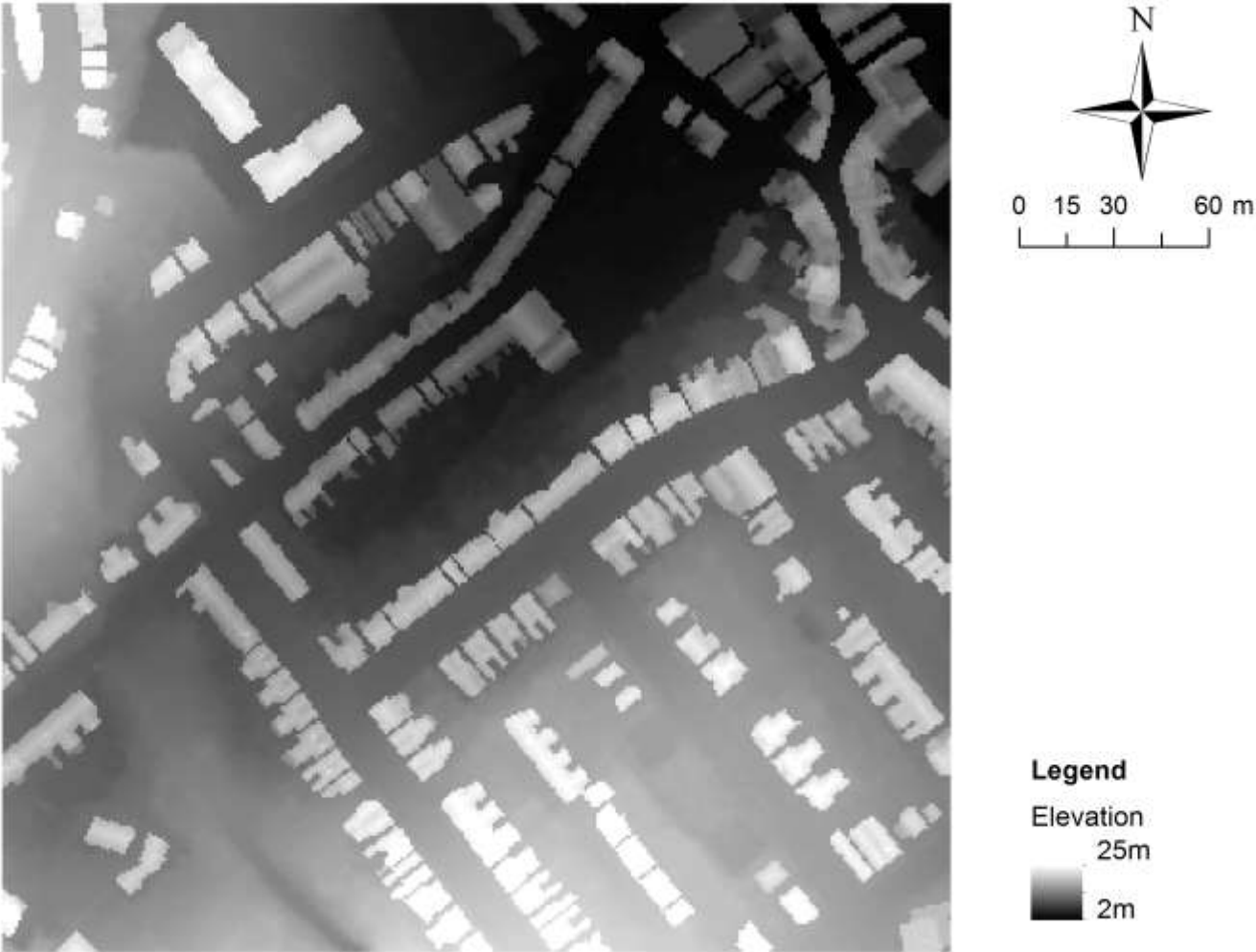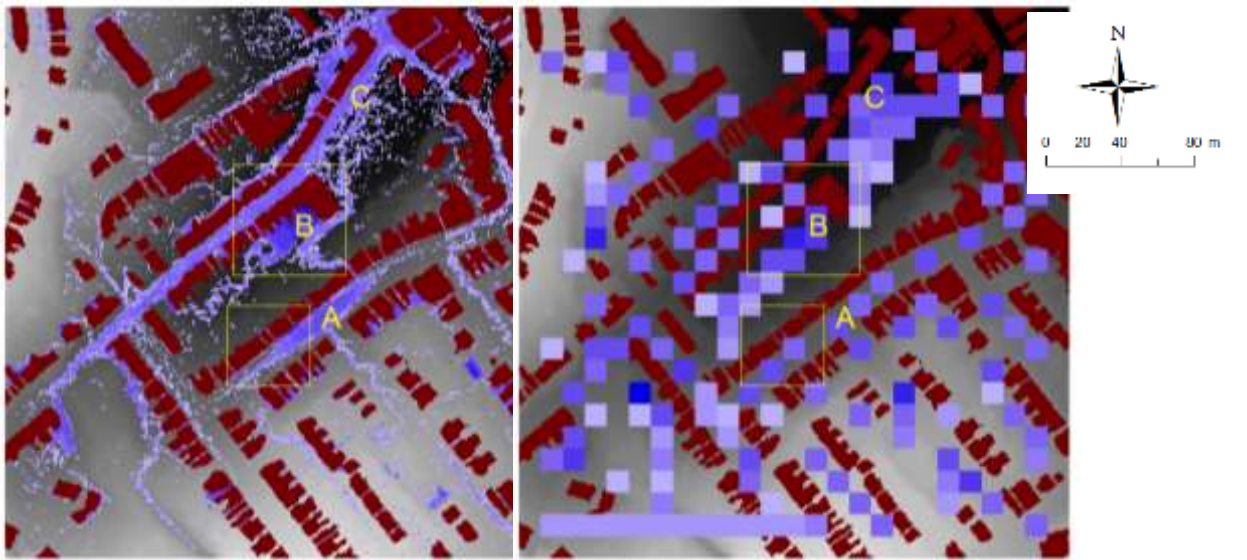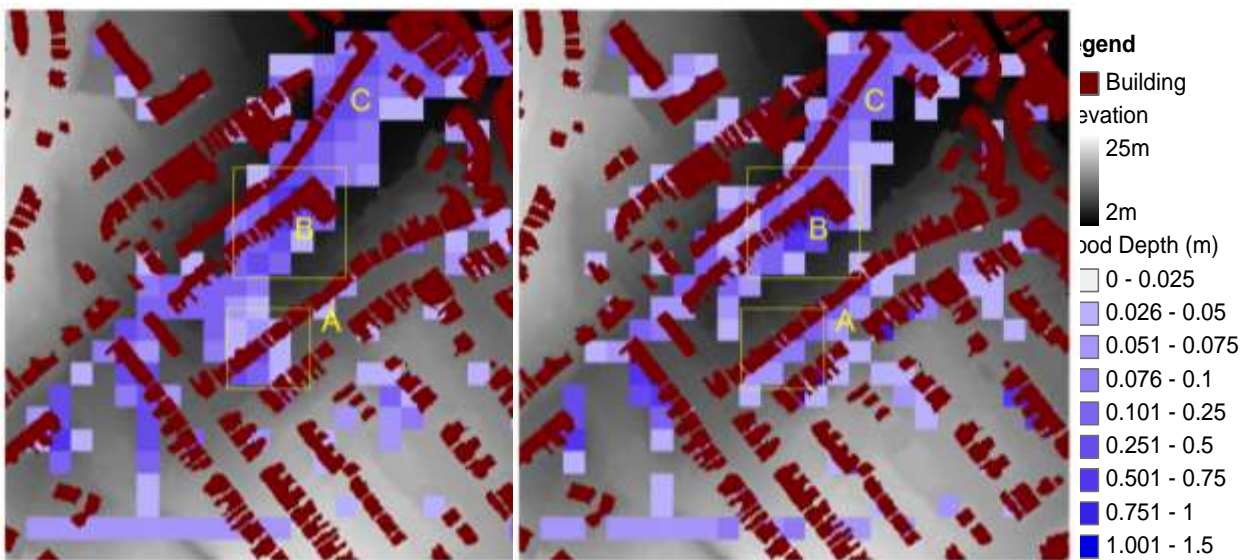
Figure 13. The terrain elevation with building height from LiDAR data for the real case study

(a) Benchmark   (b) Averaged DEM

(c) Single layer   (d) Multi-layered

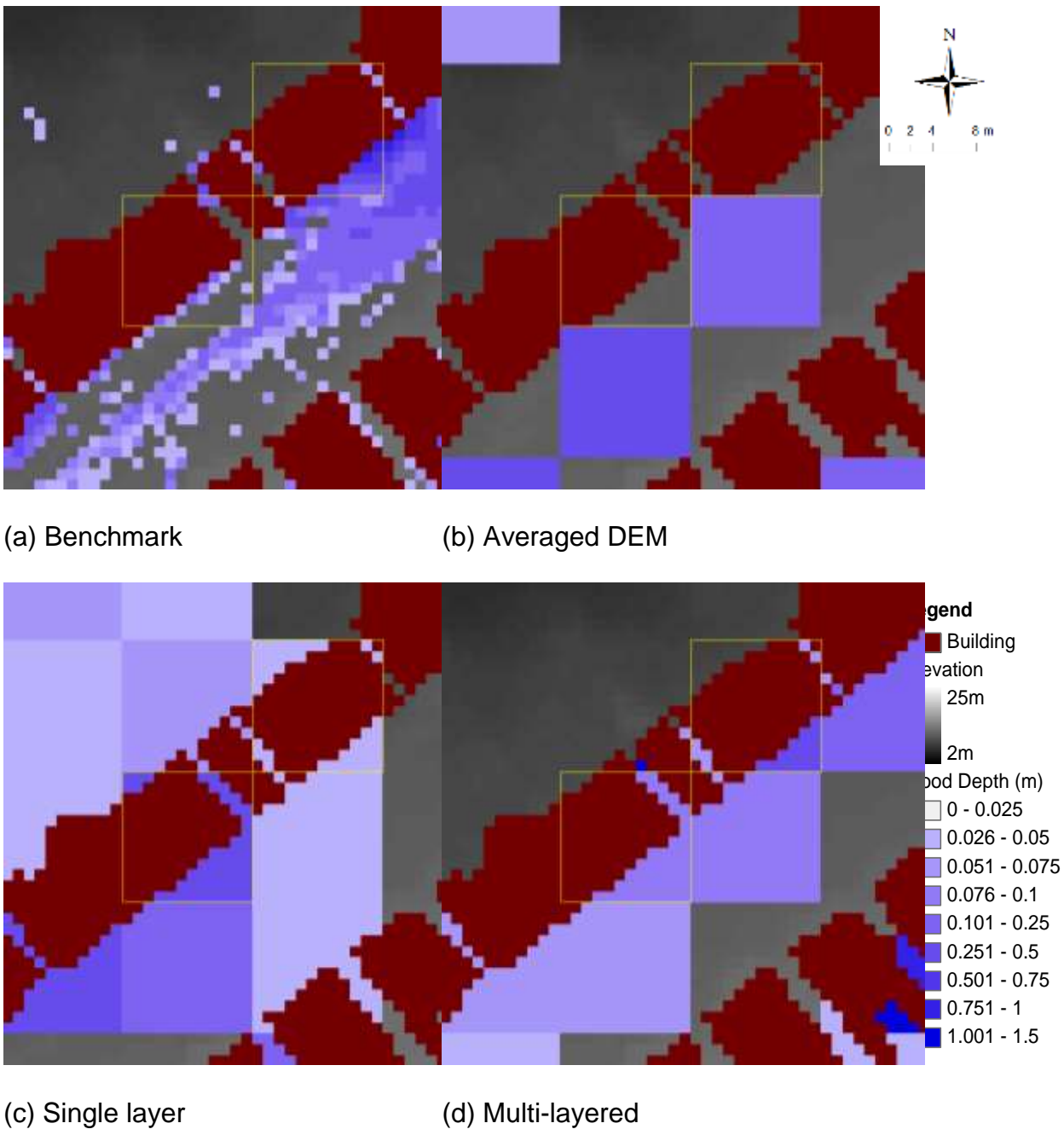Figure 14. The maximum flood depth for the benchmark and the three grid coarsening models of the real case study

(a) Benchmark   (b) Averaged DEM

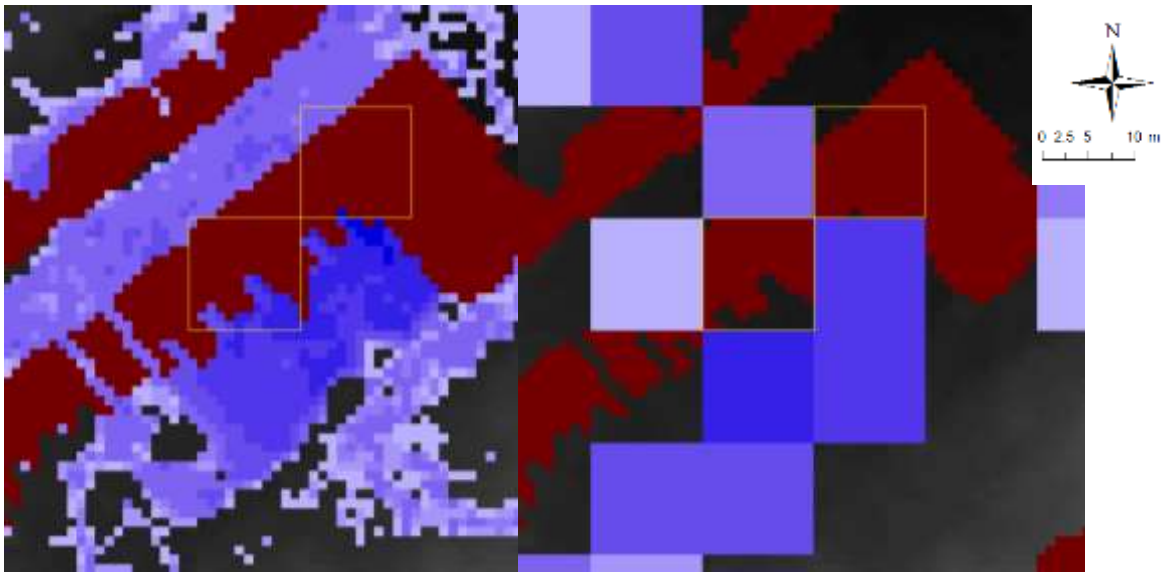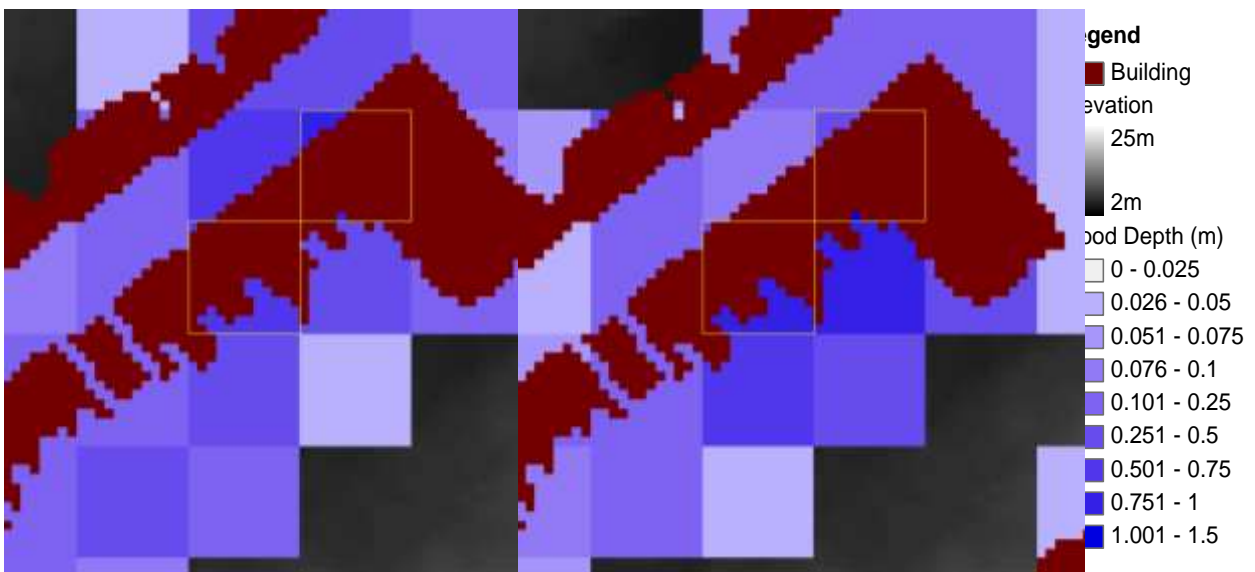(c) Single layer   (d) Multi-layered

Figure 15. The maximum flood depth for the benchmark and the three grid coarsening models of in the upstream end of region A shown in Figure 13

(a) Benchmark

(b) Averaged DEM

(c) Single layer

(d) Multi-layered

Figure 16. The maximum flood depth for the benchmark and the three grid coarsening models of in the region B shown in Figure 13